Constraints on Spin-Spin Velocity-Dependent Interactions

Wei Ji,[1,2,3] Weipeng Li,[2] Pavel Fadeev,[1,3] Filip Ficek,[4] Jianan Qin,[1,5] Kai Wei,[6,7,8,*]
Yong-Chun Liu,[2,9,†] and Dmitry Budker[1,3,10]

[1]*Helmholtz-Institut, GSI Helmholtzzentrum für Schwerionenforschung, Mainz 55128, Germany*
[2]*State Key Laboratory of Low-Dimensional Quantum Physics, Department of Physics, Tsinghua University, Beijing 100084, China*
[3]*Johannes Gutenberg-Universität Mainz, Mainz 55128, Germany*
[4]*Institute of Theoretical Physics, Jagiellonian University, Łojasiewicza 11, 30-348 Kraków, Poland*
[5]*Key Laboratory of Geophysical Exploration Equipment, Ministry of Education of China, Jilin University, Changchun 130012, China*
[6]*School of Instrumentation Science and Opto-electronics Engineering, Beihang University, Beijing 100191, China*
[7]*Hangzhou Innovation Institute, Beihang University, Hangzhou 310051, China*
[8]*Hangzhou Extremely Weak Magnetic Field Major Science and Technology Infrastructure Research Institute, Hangzhou 310051, China*
[9]*Frontier Science Center for Quantum Information, Beijing 100084, China*
[10]*Department of Physics, University of California, Berkeley, California 94720-7300, USA*

(Received 21 November 2022; revised 14 February 2023; accepted 23 February 2023; published 28 March 2023)

The existence of exotic spin-dependent forces may shine light on new physics beyond the standard model. We utilize two iron shielded $SmCo_5$ electron-spin sources and two optically pumped magnetometers to search for exotic long-range spin-spin velocity-dependent force. The orientations of spin sources and magnetometers are optimized such that the exotic force is enhanced and common-mode noise is effectively subtracted. We set direct limit on proton-electron interaction in the force range from 1 cm to 1 km. Our experiment represents more than 10 orders of magnitude improvement than previous works.

DOI: 10.1103/PhysRevLett.130.133202

The nature of dark matter is one of the most profound mysteries in modern physics. Many new light bosons introduced by theories beyond the standard model are proposed to be dark matter candidates, such as spin-0 bosons including axions and axionlike particles [1–3], spin-1 bosons including dark photons [4,5], and Z' bosons [6,7]. Furthermore, the new bosons may mediate new types of long-range fundamental forces (independent of whether they are constituents of dark matter or not) [8–11].

If we consider the spin, relative position, and velocity of two fermions, the exotic interaction between them can be classified to 16 terms [9,10], and then generally classified into static terms and velocity-dependent terms. A conventional velocity-dependent force in classical physics is the Lorentz force of a moving charged particle.

Many experimental methods have been used to search for exotic forces [12], including experiments with torsional resonators [13–16], nuclear magnetic resonance [17–20], magnetometers based on hot atoms and nitrogen-vacancy center in diamond [21–27], and other high-sensitivity technologies [28–32]. Most of these efforts focus on static interactions, while the velocity-dependent interactions have also been gaining attention in recent years [23–25,27,33,34].

In this experiment, we focus on one term of spin-spin velocity-dependent interaction (SSVDI) proposed by Ref. [9]:

$$V_8 = \frac{f_8^{12}\hbar}{4\pi c}[(\hat{\boldsymbol{\sigma}}_1 \cdot \boldsymbol{v})(\hat{\boldsymbol{\sigma}}_2 \cdot \boldsymbol{v})]\frac{e^{-r/\lambda}}{r}, \tag{1}$$

where f_8^{12} is a dimensionless coupling coefficient (the subscript 8 refers to the term V_8 from Ref. [9] and the superscripts 1,2 denote the fermion 1 and fermion 2), $\hat{\boldsymbol{\sigma}}_1$, $\hat{\boldsymbol{\sigma}}_2$ are the respective Pauli spin-matrix vectors of the two fermions, r and $\boldsymbol{v}$ are the relative position and velocity between two fermions, $\lambda = 1/m_0$ is the force range, and m_0 is the mass of the mediator boson. If the mediator of the SSVDI is a spin-1 boson such as Z', which is a dark matter candidate and may resolve other discrepancies such as that in the anomalous magnetic moment of the muon [6,35], the coupling coefficient can be rewritten as $f_8^{ep} = -g_A^e g_A^p/2$ [9,10]. To search for this force, a spin polarized test object is required as the spin source, and an ultrasensitive magnetometer is required as the sensor.

In this experiment, the spin sources are two iron shielded $SmCo_5$ magnets (ISSCs) that have high net electron spin and small magnetic leakage [36]. The sensor is a pair of optically pumped magnetometers (OPMs), in which atomic spins are optically polarized and read out, and the magnetic field is determined via its effect on the spins, which, in the simplest case, is Larmor precession. The OPMs use Rb atoms and operate in the spin-exchange relaxation-free mode [37,38]. The experimental setup is designed to be sensitive to the exotic force, while common-mode noise is

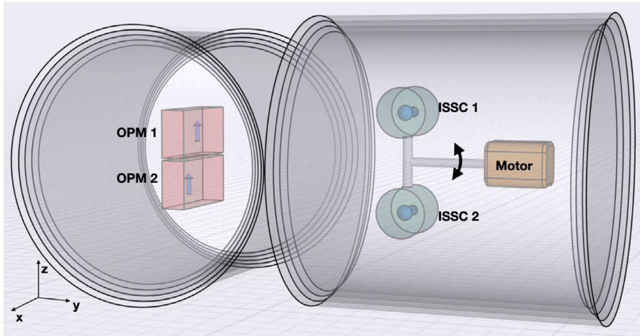

FIG. 1. The experimental setup (not to scale). Two QuSpin OPMs noted as OPM1 and OPM2 are enclosed in a five-layer magnetic shield. Their sensitive axis orientations are antiparallel along the $\hat{x}$ axis. Two spin sources noted as $ISSC_{1,2}$ are put in the other, four-layer shield. The spin source is driven with a motor to rotate clockwise or counterclockwise. The blue arrows show the direction of net spin in OPMs and ISSCs.

reduced. Our experiment sets new limits on exotic SSVDI for electron-proton coupling.

Figure 1 shows a schematic of the experimental setup. Each of the two spin sources $ISSC_{1,2}$ contains a 40-mm-diameter, 40-mm-long cylindrical $SmCo_5$ magnet enclosed in three layers of pure iron (15, 5, 5 mm thickness from inside to outside with 5 mm gaps). The magnetization of the $SmCo_5$ magnets is about 1 T. The magnetic field of the magnet is shielded by the iron layers, and the magnetic leakage outside the iron layers is smaller than 10 μT. However, the net spin of the ISSCs is not canceled, which is mostly due to the fact that the orbital magnetic moment and spin magnetic moments of the $4f$ rare earth metal (Sm) and $3d$ metals (Co and Fe) are differently oriented, and thus the total magnetic moments are canceled, but the net orbital magnetic moment and spin magnetic moment are not [13,36]. The net electron spin for each ISSC is $1.75(21) \times 10^{24}$ [36]. The ISSCs are connected with titanium-alloy supports and are driven with a motor to rotate clockwise (CW) and counterclockwise (CCW). The motor frequency is controlled with a direct current (dc) power supply.

The OPMs are QuSpin vector zero-field magnetometers (QZFM Gen-2) [39] placed in the center of a five-layer μ-metal magnetic shield. The arrows along the $\hat{z}$ axis demonstrate the direction of the circularly polarized laser beam in the position of the ^{87}Rb vapor cell. The $\hat{x}$ axis is the OPM's sensitive axis. Because the orientation of two OPMs along $\hat{x}$ is antiparallel, their responses to the magnetic field have opposite signs. If there is a magnetic field B_0 applied, the responses of the OPMs are $S_1 = B_0 + N_C + N_1$ and $S_2 = -B_0 + N_C + N_2$, respectively, where N_C is the common-mode noise and N_1 and N_2 are other noises. Subtracting the readings of the two sensors can diminish the common noise and yields a signal of $S_{\mathrm{sub}} = (S_1 - S_2)/2 = B_0 + (N_1 - N_2)/2$.

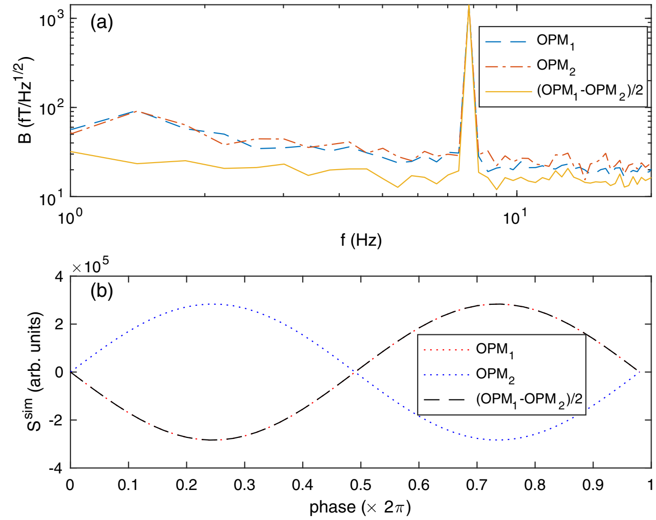

FIG. 2. Top: a typical spectrum of two OPMs and the subtraction result. A uniform ac magnetic field of 8 Hz is applied along the $\hat{x}$ axis. The dashed blue line and the red dot-dashed line are the spectrum of the OPMs on the left-hand and right-hand side, respectively. The yellow solid line is their difference. Bottom: the OPMs' response to the pseudomagnetic field along the $\hat{x}$ axis. The blue dotted and red dotted line are the pseudomagnetic field sensed by OPM_1 and OPM_2, respectively, and the black dashed line is the subtraction result. The subtraction result agrees well with the result from OPM_1.

To test the validity of the subtraction procedure, an 8 Hz and 1.5 pT uniform magnetic field is applied along $\hat{x}$ with a set of Helmholtz coils. The spectrum of the OPM signals and the subtraction result are shown in Fig. 2(a). By taking the difference, the uniform magnetic field is unaffected, the common-mode (for example, electrical or gradient) noise is reduced by as high as a factor of 5, and the 8 Hz target signal is successfully extracted. The noise level around 8 Hz is about 13 $\mathrm{fT}/\sqrt{\mathrm{Hz}}$.

The SSVDIs will manifest as pseudomagnetic fields that could be sensed by the Rb atoms like the Zeeman effect. The potential can be expressed as $V_8^n \zeta^n + V_8^p \zeta^p + V_8^e \zeta^e = -\boldsymbol{\mu} \cdot \mathbf{B}$, where $\boldsymbol{\mu}$ is the magnetic moment of the Rb atom, $\mathbf{B}$ is the pseudomagnetic field from the exotic interaction, and $\zeta^{n,p,e}$ are the neutron, proton, and electron's fraction of spin polarization in ^{87}Rb atoms, which could be obtained by the Russel-Saunders LS coupling and the Schmidt model of nuclear physics.

In this experiment, we search for the coupling between the proton, neutron, and electron spins in the Rb atoms and the electron spins in ISSCs. The pseudomagnetic field sensed by the OPM can be obtained by integrating the exotic interaction from the electron spins over the ISSCs:

$$\boldsymbol{B}^{p,e,n} = \frac{f_8 \zeta^{p,e,n} \hbar}{4\pi\mu c} \iiint \rho(\boldsymbol{r})(\hat{\boldsymbol{\sigma}}_2 \cdot \boldsymbol{v}) \frac{\boldsymbol{v}}{r} e^{-r/\lambda} d\boldsymbol{r}, \qquad (2)$$

where $\mathbf{B}^{p,n,e}$ are the fractions of $\mathbf{B}$ that couple to proton, neutron, and electron, respectively, $\boldsymbol{v}(\boldsymbol{r}) = \boldsymbol{\omega} \times \boldsymbol{r}$ and $\rho(\boldsymbol{r})$

are the velocity and spin density at location $\boldsymbol{r}$, and $\boldsymbol{\omega}$ is the angular velocity of the ISSCs. The proton and electron fractions of polarization in ^{87}Rb are $\zeta^p = 0.29$ and $\zeta^e = 0.13$, respectively, and neutron polarization ζ^n is assumed to be zero under the basic nuclear shell model. The calculation of the fraction of spin polarization is explained in the Supplemental Material [40], which includes Refs. [41,42].

The experimental parameters and a benchmark coupling coefficients $f_8^0 = 1$ are put in the simulation to obtain $\mathbf{B}^p$. The benchmark parameter $f_8^0 = 1$ is set to 1 for convenience; a different $f_8^0 = 1$ does not affect the final result. The orientation of the OPMs and ISSC sources is optimized by simulating different configurations, such that the OPMs can sense the maximum pseudomagnetic field. The best configuration is shown in Fig. 1 and Table I. The speed of the centers of the ISSCs is $v = 2\pi f D/2 \approx 3.2$ m/s, where D is the distance between ISSCs' centers and f is the rotation frequency. The distance between the spin sources and the OPMs is much larger than the distance between two OPMs, such that two OPMs experience almost the same pseudomagnetic field. Thus the signal subtraction procedure works well for this pseudomagnetic field. The simulated responses of the two OPMs and their subtraction result are shown in Fig. 2(b).

The ISSC spin sources are driven with a dc motor. The positions of the spin sources are monitored with a photoelectronic encoder placed on the rotation axle. The signals of the encoder and the OPMs are taken simultaneously and recorded with a data-acquisition device. The motor is tuned to rotate CCW and CW alternatively for every 2 h. The dc motor works in a good stability with frequency of 4.09(1) and 4.11(1) Hz for CW and CCW rotations.

The two OPMs' signals are subtracted and then transformed to frequency domain by fast Fourier transformations (FFT). The 50 Hz power line interference and its 100 and 200 Hz harmonics are removed in the frequency domain. The data were then transformed back to the time domain with inverse FFT.

The signals are then cut to one-period-long segments based on the encoder signal of the spin source rotation. The dc components in each period are removed. The data are noted as $\boldsymbol{S}_i^{\exp}(t_j)$, where i represents the ith period and t_j is the time of the jth point in this period.

The coupling coefficient f_8^{ep} can be obtained by a similarity comparison method between the experimental data and simulation results:

$$f_{8,i}^{ep} = k_i \sqrt{\frac{\sum_j [\boldsymbol{S}_i^{\exp}(t_j)]^2}{\sum_j [\boldsymbol{S}^{\mathrm{sim}}(t_j)]^2}}, \tag{3}$$

where k_i is the similarity score to weigh the similarity between $\boldsymbol{S}_i^{\exp}$ and $\boldsymbol{S}^{\mathrm{sim}}(t)$ [43], which is defined as

$$k_i \equiv \frac{\sum_j \boldsymbol{S}^{\mathrm{sim}}(t_j) \cdot \boldsymbol{S}_i^{\exp}(t_j)}{\sqrt{\sum_j [\boldsymbol{S}^{\mathrm{sim}}(t_j)]^2} \sqrt{\sum_j [\boldsymbol{S}_i^{\exp}(t_j)]^2}}. \tag{4}$$

The expectation values and standard error for the CW and CCW rotation are $\langle f_8^{ep} \rangle^+$, $\langle f_8^{ep} \rangle^-$ and σ^+, σ^-, respectivly, and the final coupling coefficient can be obtained by

$$\langle f_8^{ep} \rangle = \frac{\langle f_8^{ep} \rangle^+ / \sigma^{+^2} + \langle f_8^{ep} \rangle^- / \sigma^{-^2}}{1/\sigma^{+^2} + 1/\sigma^{-^2}}. \tag{5}$$

Some systematic bias could be removed by averaging over CW and CCW. The distributions of the f_8^{ep+} and f_8^{ep-} are shown in Fig. 3.

We first choose a force range $\lambda = 20$ m to demonstrate the sensitivity. The parameters of the experiment and their

TABLE I. Experimental parameters and the error budget of f_8^{ep}. The origin of coordinates is at the midpoint between the centers of the two OPMs. The contributions to the error budget are evaluated for $\lambda = 20$ m. The final systematic error is derived from the uncertainties of the parameters listed.

Parameter	Value	$\Delta f_8^{ep} (\times 10^{-22})$
ISSC net spin ($\times 10^{24}$)	1.75(21)	0.084
Position of ISSCs x (m)	0.000(2)	0.001
Position of ISSCs y (m)	−0.477(2)	0.001
Position of ISSCs z (m)	0.000(2)	0.001
Distance between ISSC centers (m)	0.251(1)	0.044
Distance between OPM cells (m)	0.017(1)	0.004
Rotation frequency CW (Hz)	4.11(1)	
Rotation frequency CCW (Hz)	4.09(1)	
Phase uncertainty (deg)	±2.8	±1.190
Final $f_8^{\exp}$ ($\times 10^{-22}$) ($\lambda = 20$ m)	−0.7	±10.1 (stat) ±1.2 (syst)

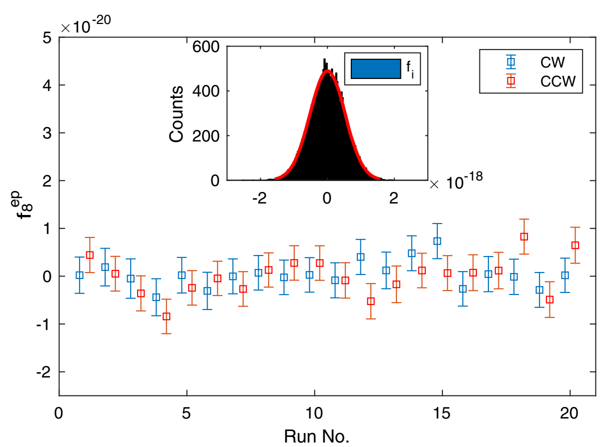

FIG. 3. Statistical results of the f_8^{ep}. Each data point represents an average of about one 2.7-h-long dataset. The distribution of f_8^{ep} for one dataset is shown in the inset. The result is well fitted with a Gaussian distribution (red line) with $\bar{\chi}^2 = 1.18$.

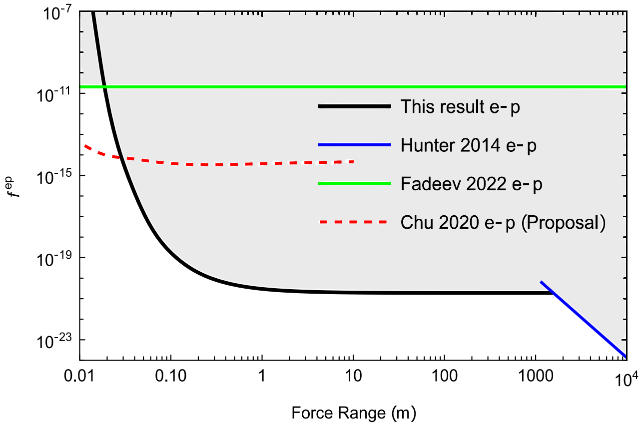

FIG. 4. Limits on the SSVDI coupling coefficients between electron and proton. The black solid line is our constraints. "Hunter2014 e-p" is from Ref. [24] that uses geoelectrons and atomic magnetometer; "Fadeev 2022 e-p" is from Ref. [44] that compares the experimental and theoretical results of hydrogen spectroscopy; "Chu 2020 e-p" [45] propose to use ^{3}He as sensor and dysprosium iron garnet as spin source, the line is based on their sensitivity at 3×10^{-17} T and is rescaled using the fraction of spin polarization $\zeta_p^{^3\mathrm{He}} = -0.027$ [46].

corresponding uncertainties on $\Delta f_8^{\mathrm{exp}}$ are shown in Table I. The f_8^{ep} is determined to be $f_8^{ep} = 0.7 \pm 10.1_{\mathrm{stat}} \pm 1.2_{\mathrm{syst}} (\times 10^{-22})$. No evidence of the SSVDI is observed. New constraints on the f between electron-proton is set to be $|f_8^{ep}| \le 2.0\times10^{-21}$ by the 95% confidence level, where to set the limit on one of these coupling-constant products, we assume that the other one is zero. For instance, the f^{ep} constraints are set assuming electron-neutron and electron-electron contributions to the signal are zero. This result represents a limit on $|g_A^e g_A^p| \le 4.0\times10^{-21}$. Note that the velocity-independent term provides significantly tighter limit on $g_A g_A$ coefficients [9,10]; however, the SSVDI provides a unique way to explore the velocity-dependent interactions. The values for other λ's are obtained with the same procedure, and the final limits are shown in Fig. 4.

A comparison between our results (black and dashed red lines) and the literature is shown in Fig. 4. With the same hydrogen-spectrum analysis used in Ref. [44], we obtained a bound on the SSVDI of $|f_8^{ep}| < 2.0\times10^{-11}$ for the range larger than 1 cm (the green line "Fadeev 2022 e-p" in Fig. 4). The ferromagnetic shielding can suppress the effect of pseudomagnetic field for the electron-electron coupling because the electron spin in the shielding is also affected by the exotic field [47]. We thus do not consider the electron-electron term in this Letter. Results on the couplings between other fermions, such as the coupling between electron-electron [22,24,30] neutron-proton [48], and electron-antiproton [49] are not plotted in Fig. 4.

The major advance of our experiment is that the ISSC spin sources have much larger numbers of spins compared to those in precision-spectroscopy experiments yielding data for the analyses in Refs. [30,49] and spin-exchange approaches [48], which are most sensitive to forces with ranges on the atomic to microscopic scale. The other advantage is that the OPMs typically have energy resolution on the order of 10^{-18} eV [41], significantly better than for the spectroscopy used in Refs. [30,49]. On the other hand, spectroscopy experiments have an advantage over macroscopic once in the short range, because of the exponential decay of the exotic force. Our search covers the range of parameters inaccessible for the geoelectron experiment [24]. Using the same method and data, we also set limits for the electron-proton coupling on the V_{6+7}, V_{15}, and V_{16} terms of SSVDF [9,10]. The results are shown in the Supplemental Material [40], which includes Refs. [9,24,45,50].

A major concern in this experiment was magnetic leakage from the ISSCs. With the iron shielding, at a distance of 10 cm away from the ISSC's surface, its residual magnetic field was measured to be less than 10 μT. The shielding factors for the magnetic shielding of both the ISSCs and OPMs were measured to be greater than 10^6. Considering all the decay and shielding factors, we conservatively expect the magnetic leakage from the ISSCs to the position of the OPMs to be smaller than 0.1 aT, which was insignificant with regards to the error budget.

The stability of the OPM is monitored throughout the experiment. The dc drift of the OPM is less than 2 pT within 2 h. A servo motor has a better frequency precision; however, commercial servo motor's control systems have electromagnetic coupling with the magnetometer [22]. A dc motor is chosen to diminish this coupling. The experiment can further be improved if a larger size ISSC could be used. The vapor cell can also be replaced with a magnetometer that uses a levitated ferromagnetic sphere and has orders of magnitude better potential magnetic sensitivity [51].

In summary, we utilized a pair of OPMs that can reduce the common noise and have ultrahigh sensitivity to search for exotic spin-dependent physics. Together with the high electron spin density iron shielded $SmCo_5$ spin source, the new experiment sets new limits on SSVDI, with more than 10 orders of magnitude improvement for the electron-proton coupling.

We thank Dr. Derek F. Jackson Kimball and Dr. Changbo Fu for valuable discussions. This work is supported by Key-Area Research and Development Program of Guangdong Province (Grant No. 2019B030330001), the National Natural Science Foundation of China (NSFC) (Grants No. 12275145, No. 92050110, No. 91736106, No. 11674390, and No. 91836302), and the National Key R&D Program of China (Grant No. 2018YFA0306504), the DFG Project No. 390831469: EXC 2118 (PRISMA+ Cluster of Excellence), by the German Federal Ministry of Education and Research (BMBF) within the Quantumtechnologien program (Grant No. 13N15064), by the QuantERA project LEMAQUME (DFG Project No. 500314265), and by COST Action COSMIC WISPers CA21106, supported by COST (European Cooperation in Science and Technology).

*weikai@buaa.edu.cn
†ycliu@tsinghua.edu.cn

[1] R. D. Peccei and H. Quinn, *CP* Conservation in the Presence of Pseudoparticles, Phys. Rev. Lett. **38**, 1440 (1977).
[2] J. Preskill, M. B. Wise, and F. Wilczek, Cosmology of the invisible axion, Phys. Lett. **120B**, 127 (1983).
[3] P. W. Graham, I. G. Irastorza, S. K. Lamoreaux, A. Lindner, and K. A. van Bibber, Experimental searches for the axion and axion like particles, Annu. Rev. Nucl. Part. Sci. **65**, 485 (2015).
[4] J. Jaeckel and A. Ringwald, The low-energy frontier of particle physics, Ann. Rev. Nucl. Part. Sci **60**, 405 (2010).
[5] H. An, M. Pospelov, J. Pradler, and A. Ritz, Direct detection constraints on dark photon dark matter, Phys. Lett. B **747**, 331 (2015).
[6] N. Okada, S. Okada, D. Raut, and Q. Shafi, Dark matter Z' and XENON1T excess from $U(1)_x$ extended standard model, Phys. Lett. B **810**, 135785 (2020).
[7] D. Croon, G. Elor, R. K. Leane, and S. D. McDermott, Supernova muons: New constraints on Z' bosons, axions and ALPs, J. High Energy Phys. 01 (2021) 107.
[8] J. Moody and F. Wilczek, New macroscopic forces?, Phys. Rev. D **30**, 130 (1984).
[9] B. A. Dobrescu and I. Mocioiu, Spin-dependent macroscopic forces from new particle exchange, J. High Energy Phys. 11 (2006) 005.
[10] P. Fadeev, Y. V. Stadnik, F. Ficek, M. G. Kozlov, V. V. Flambaum, and D. Budker, Revisiting spin-dependent forces mediated by new bosons: Potentials in the coordinate-space representation for macroscopic- and atomic-scale experiments, Phys. Rev. A **99**, 022113 (2019).
[11] P. Fayet, The fifth interaction in grand-unified theories: A new force acting mostly on neutrons and particle spins, Phys. Lett. B **172**, 363 (1986).
[12] M. Safronova, D. Budker, D. DeMille, D. F. Jackson Kimball, A. Derevianko, and C. W. Clark, Search for new physics with atoms and molecules, Rev. Mod. Phys. **90**, 025008 (2018).
[13] B. R. Heckel, E. G. Adelberger, C. E. Cramer, T. S. Cook, S. Schlamminger, and U. Schmidt, Preferred-frame and *CP*-violation tests with polarized electrons, Phys. Rev. D **78**, 092006 (2008).
[14] G. D. Hammond, C. C. Speake, C. Trenkel, and A. P. Patón, New Constraints on Short-Range Forces Coupling Mass to Intrinsic Spin, Phys. Rev. Lett. **98**, 081101 (2007).
[15] J. Long, H. W. Chan, A. B. Churnside, E. A. Gulbis, M. C. M. Varney, and J. C. Price, Upper limits to submillimetre-range forces from extra space-time dimensions, Nature (London) **421**, 922 (2003).
[16] W. Terrano, E. Adelberger, J. Lee, and B. Heckel, Short-Range, Spin-Dependent Interactions of Electrons: A Probe for Exotic Pseudo-Goldstone Bosons, Phys. Rev. Lett. **115**, 201801 (2015).
[17] A. Petukhov, G. Pignol, D. Jullien, and K. Andersen, Polarized ^{3}He as a Probe for Short-Range Spin-Dependent Interactions, Phys. Rev. Lett. **105**, 170401 (2010).
[18] H. Yan, G. A. Sun, S. M. Peng, Y. Zhang, C. Fu, H. Guo, and B. Q. Liu, Searching for New Spin- and Velocity-Dependent Interactions by Spin Relaxation of Polarized ^{3}He Gas, Phys. Rev. Lett. **115**, 182001 (2015).
[19] P.-H. Chu *et al.*, Laboratory search for spin-dependent short-range force from axionlike particles using optically polarized ^{3}He gas, Phys. Rev. D **87**, 011105(R) (2013).
[20] A. Arvanitaki and A. A. Geraci, Resonantly Detecting Axion-Mediated Forces with Nuclear Magnetic Resonance, Phys. Rev. Lett. **113**, 161801 (2014).
[21] G. Vasilakis, J. M. Brown, T. W. Kornack, and M. V. Romalis, Limits on New Long Range Nuclear Spin-Dependent Forces Set with a $\mathbf{K}-{}^3$He Comagnetometer, Phys. Rev. Lett. **103**, 261801 (2009).
[22] W. Ji, Y. Chen, C. Fu, M. Ding, J. Fang, Z. Xiao, K. Wei, and H. Yan, New Experimental Limits on Exotic Spin-Spin-Velocity-Dependent Interactions by Using $SmCo_5$ Spin Sources, Phys. Rev. Lett. **121**, 261803 (2018).
[23] M. Jiao, M. Guo, X. Rong, Y.-F. Cai, and J. Du, Experimental Constraint on an Exotic Parity-Odd Spin- and Velocity-Dependent Interaction with a Single Electron Spin Quantum Sensor, Phys. Rev. Lett. **127**, 010501 (2021).
[24] L. Hunter and D. Ang, Using Geoelectrons to Search for Velocity-Dependent Spin-Spin Interactions, Phys. Rev. Lett. **112**, 091803 (2014).
[25] H. Su, Y. Wang, M. Jiang, W. Ji, P. Fadeev, D. Hu, X. Peng, and D. Budker, Search for exotic spin-dependent interactions with a spin-based amplifier, Sci. Adv. **7**, eabi9535 (2021).
[26] A. Almasi, J. Lee, H. Winarto, M. Smiciklas, and M. V. Romalis, New Limits on Anomalous Spin-Spin Interactions, Phys. Rev. Lett. **125**, 201802 (2020).
[27] Y. J. Kim, P.-H. Chu, and I. Savukov, Experimental Constraint on an Exotic Spin- and Velocity-Dependent Interaction in the sub-MeV Range of Axion Mass with a Spin-Exchange Relaxation-Free Magnetometer, Phys. Rev. Lett. **121**, 091802 (2018).
[28] K. Tullney *et al.*, Constraints on Spin-Dependent Short-Range Interaction between Nucleons, Phys. Rev. Lett. **111**, 100801 (2013).
[29] A. P. Serebrov *et al.*, Search for macroscopic *CP* violating forces using a neutron EDM spectrometer, JETP Lett. **91**, 6 (2010).
[30] F. Ficek, D. F. Jackson Kimball, M. G. Kozlov, N. Leefer, S. Pustelny, and D. Budker, Constraints on exotic spin-dependent interactions between electrons from helium fine-structure spectroscopy, Phys. Rev. A **95**, 032505 (2017).
[31] X. Ren, J. Wang, R. Luo, L. Yin, J. Ding, G. Zeng, and P. Luo, Search for an exotic parity-odd spin- and velocity-dependent interaction using a magnetic force microscope, Phys. Rev. D **104**, 032008 (2021).
[32] Y. Stadnik, V. Dzuba, and V. Flambaum, Improved Limits on Axionlike-Particle-Mediated p, t-Violating Interactions between Electrons and Nucleons from Electric Dipole Moments of Atoms and Molecules, Phys. Rev. Lett. **120**, 013202 (2018).

[33] K. Wei, W. Ji, C. Fu, A. Wickenbrock, V. V. Flambaum, J. Fang, and D. Budker, New constraints on exotic spin-velocity-dependent interactions, Nat. Commun. **13**, 7387 (2022).

[34] P. Malta, L. Ospedal, K. Veiga, and J. Helayël-Neto, Comparative aspects of spin-dependent interaction potentials for spin-$1/2$ and spin-1 matter fields, Adv. High Energy Phys. **2016**, 2531436 (2016).

[35] B. Arushi and C. Rupert, Solving the electron and muon $g-2$ anomalies in Z' models, Eur. Phys. J. C **81**, 1065 (2021).

[36] W. Ji, C. Fu, and H. Gao, Searching for new spin-dependent interactions with $SmCo_5$ spin sources and a spin-exchange-relaxation-free comagnetometer, Phys. Rev. D **95**, 075014 (2017).

[37] J. Allred, R. Lyman, T. Kornack, and M. V. Romalis, High-Sensitivity Atomic Magnetometer Unaffected by Spin-Exchange Relaxation, Phys. Rev. Lett. **89**, 130801 (2002).

[38] V. Shah, S. Knappe, P. D. Schwindt, and J. Kitching, Subpicotesla atomic magnetometry with a microfabricated vapour cell, Nat. Photonics **1**, 649 (2007).

[39] QuSpin, GZFM Gen-2, http://quspin.com/products-qzfm, accessed April 3, 2021.

[40] See Supplemental Material at http://link.aps.org/supplemental/10.1103/PhysRevLett.130.133202 for details of the fraction of spin polarisation and the limits on other terms of spin-spin velocity-dependent forces.

[41] D. J. Kimball, Nuclear spin content and constraints on exotic spin-dependent couplings, New J. Phys. **17**, 073008 (2015).

[42] I. Savukov and M. Romalis, Effects of spin-exchange collisions in a high-density alkali-metal vapor in low magnetic fields, Phys. Rev. A **71**, 023405 (2005).

[43] A. S. Krasichkov, E. B. Grigoriev, M. I. Bogachev, and E. M. Nifontov, Shape anomaly detection under strong measurement noise: An analytical approach to adaptive thresholding, Phys. Rev. E **92**, 042927 (2015).

[44] P. Fadeev, F. Ficek, M. G. Kozlov, D. Budker, and V. V. Flambaum, Pseudovector and pseudoscalar spin-dependent interactions in atoms, Phys. Rev. A **105**, 022812 (2022).

[45] P.-H. Chu, Y. Kim, and I. Savukov, Search for exotic spin-dependent interactions using polarized helium, arXiv:2002.02495.

[46] G. Vasilakis, J. Brown, T. Kornack, and M. Romalis, Limits on New Long Range Nuclear Spin-Dependent Forces Set with a K-^{3}He Comagnetometer, Phys. Rev. Lett. **103**, 261801 (2009).

[47] D. J. Kimball, J. Dudley, Y. Li, S. Thulasi, S. Pustelny, D. Budker, and M. Zolotorev, Magnetic shielding and exotic spin-dependent interactions, Phys. Rev. D **94**, 082005 (2016).

[48] D. J. Kimball, A. Boyd, and D. Budker, Constraints on anomalous spin-spin interactions from spin-exchange collisions, Phys. Rev. A **82**, 062714 (2010).

[49] F. Ficek, P. Fadeev, V. V. Flambaum, D. F. Jackson Kimball, M. G. Kozlov, Y. V. Stadnik, and D. Budker, Constraints on Exotic Spin-Dependent Interactions between Matter and Antimatter from Antiprotonic Helium Spectroscopy, Phys. Rev. Lett. **120**, 183002 (2018).

[50] T. Leslie, E. Weisman, R. Khatiwada, and J. Long, Prospects for electron spin-dependent short-range force experiments with rare earth iron garnet test masses, Phys. Rev. D **89**, 114022 (2014).

[51] A. Vinante, C. Timberlake, D. Budker, D. F. Jackson Kimball, A. O. Sushkov, and H. Ulbricht, Surpassing the Energy Resolution Limit with Ferromagnetic Torque Sensors, Phys. Rev. Lett. **127**, 070801 (2021).